

Raman Spectroscopy of Monolayer to Bulk PtSe₂ Exfoliated Crystals

Marin Tharrault,¹ Eva Desgué,² Dominique Carisetti,² Bernard Plaçais,¹

Christophe Voisin,¹ Pierre Legagneux,² and Emmanuel Baudin^{1,3}

¹*Laboratoire de Physique de l'Ecole normale supérieure, ENS, Université PSL, CNRS,
Sorbonne Université, Université de Paris, 24 rue Lhomond, 75005 Paris, France*

²*Thales Research & Technology, 91767 Palaiseau, France*

³*Institut universitaire de France*

Abstract

Raman spectroscopy is widely used to assess the quality of 2D materials thin films. This report focuses on PtSe₂, a noble transition metal dichalcogenide which has the remarkable property to transit from a semi-conductor to a semi-metal with increasing layer number. While polycrystalline PtSe₂ can be grown with various crystalline qualities, getting insight into the monocrystalline intrinsic properties remains challenging. We report on the study of exfoliated 1 to 10 layers PtSe₂ by Raman spectroscopy, featuring record linewidth. The clear Raman signatures allow layer-thickness identification and provides a reference metrics to assess crystal quality of grown films.

Keywords: 2D materials, TMD, PtSe₂, Raman spectroscopy, intrinsic properties, exfoliation, quality metrics

Transition Metal Dichalcogenides (TMDs) are promising materials for future electronic and optoelectronic devices, owing to their large optical absorption per layer and high electronic mobility [1, 2]. Furthermore, they feature strong van der Waals interlayer coupling, resulting in a tunable layer-dependent band structure. Among TMDs, thin films of Platinum Diselenide (1T – PtSe₂) are semi-conductors and feature exceptional bandgap variations, with a transition to a semi-metal with increasing thickness [1, 3–5]. For this reason it can reach small bandgap values, permitting efficient photodetection in the infrared range [1, 3, 6]. This makes PtSe₂ a promising building block for optoelectronic devices operating in the telecom band, and several growth methods (CVD, TAC, MBE) are being developed to provide high-quality scalable films for industry [2, 3, 7–12]. These films are commonly characterized using a variety of methods, including electron diffraction, X-ray spectroscopy or diffraction, electron microscopy, atomic force microscopy, electronic transport measurements and optical spectroscopy [2, 13].

Among these methods, Raman spectroscopy presents several key advantages: fast, cheap and non-contact, it probes optical phonon transitions – highly sensitive to defects – and is therefore used as a primary characterization to identify the structure and assess film quality [14–18]. Previous works on PtSe₂ established the most salient Raman spectral features [19–25]: they identified the optical vibrational phonon modes associated with the peaks, detailed the Raman peaks intensities and shifts evolution with the thickness, proposed quality metrics, and studied the polarization and temperature dependencies of the Raman peaks. However, due to the limited quality of the studied samples, the precise features of the Raman signature of few-layer intrinsic PtSe₂ remained out of reach.

In this work, we report high-resolution Raman spectroscopy of record-quality exfoliated PtSe₂ crystals of layer-controlled thickness. We establish criteria for film quality, and demonstrate that the characteristic Raman signature of thin flakes enables the determination of layer count. By providing reference Raman spectra of exfoliated single crystals, this work will guide the development of the continuously improving PtSe₂ growth technology [2, 8, 12].

SAMPLES FABRICATION

Chemical Vapour Transport grown PtSe₂ crystals (HQ Graphene [26]) are exfoliated on fused silica substrates, as shown in **figure 1a**. Au-assisted mechanical exfoliation provides flakes as thin as a monolayer thanks to the strong affinity of gold with Selenium atoms [27–29].

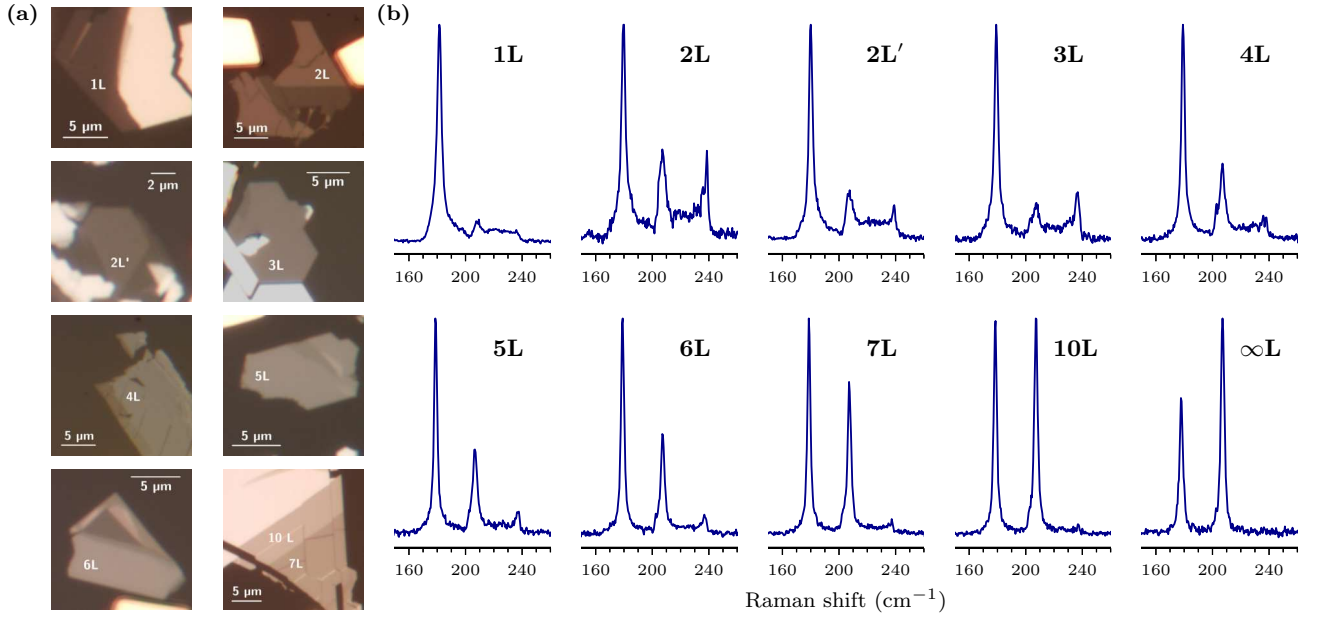


FIG. 1. PtSe₂ exfoliated flakes and their Raman spectra. (a) Micrographs of PtSe₂ flakes, each region of interest is labeled with its layer count. (b) The associated Raman spectra displayed on the 150 – 260 cm⁻¹ range, and normalized to their maximum amplitude.

Each flake number of layers is identified using absorption microspectroscopy and confirmed by Atomic Force Microscopy, as described in detail in reference [30].

ATOMIC STRUCTURE SIGNATURE

High-resolution Raman spectroscopy is performed using a 50 μ W low-power 514 nm green laser source, together with a 50 cm^{-1} edgepass filter (additional details in experimental section).

Spectra of selected flakes are displayed in figure 1b and consist in 3 solitary peaks in the 150 – 260 cm^{-1} spectral range. The flake thickness has little influence on the total scattered Raman intensity. This can be understood by the fact that green light is resonantly absorbed regardless of the number of layers [30]. The full set of spectra is included in the Supplementary Material (SM), figure 1.

The spectral shapes correspond to the 1T phase of PtSe_2 , identified with its 4 optical phonon modes: the Raman-active E_g and A_{1g} modes around 180 cm^{-1} and 210 cm^{-1} respectively, and the IR-active A_{2u} and E_u modes gathered as LO (longitudinal optical) around 230 cm^{-1} [5, 19, 31], as depicted in **figure 2a**.

Raman modes spectral weights and widths are assessed by a 4-components Lorentzian fit. Each Lorentzian function $L(\tilde{\nu})$ is parameterized by its shift $\tilde{\nu}_0$, its integrated intensity I , and full width at half maximum (thereafter abbreviated as width) Γ , such that:

$$L(\tilde{\nu}) = \frac{I}{\pi} \frac{\Gamma/2}{(\tilde{\nu} - \tilde{\nu}_0)^2 + (\Gamma/2)^2} \quad (1)$$

Selected fit parameters are gathered in figures 2b-e. More extensive data can be found in figure SM2. Furthermore, the Raman signatures are mostly uniform over the flakes surfaces (down to the measurement accuracy, SM3).

Almost all samples are identified using optical absorption spectroscopy as the most-stable AA stacking, as their optical absorption spectra match Density Functional Theory (DFT) predictions [30]. 2L' samples are a noticeable exception, with a singular Raman signature differing from the one of 2L (detailed comparison in SM4). In fact, the comparison of absorption behavior with DFT predictions for 2L' suggests an AB stacking [30], which has been theoretically identified as a stable phase for 1T – PtSe_2 [5, 30, 31], and is a common defect in grown films [12, 35, 36].

The influence of the substrate on the Raman signature is moreover investigated. We compare the Raman spectra of few-layers flakes deposited on fused silica and crystalline sapphire (figure SM5). No noticeable difference can be observed, the Raman signature appearing to be identical. It is likely due to the fact that in both cases, the flakes and the substrate are not directly in van

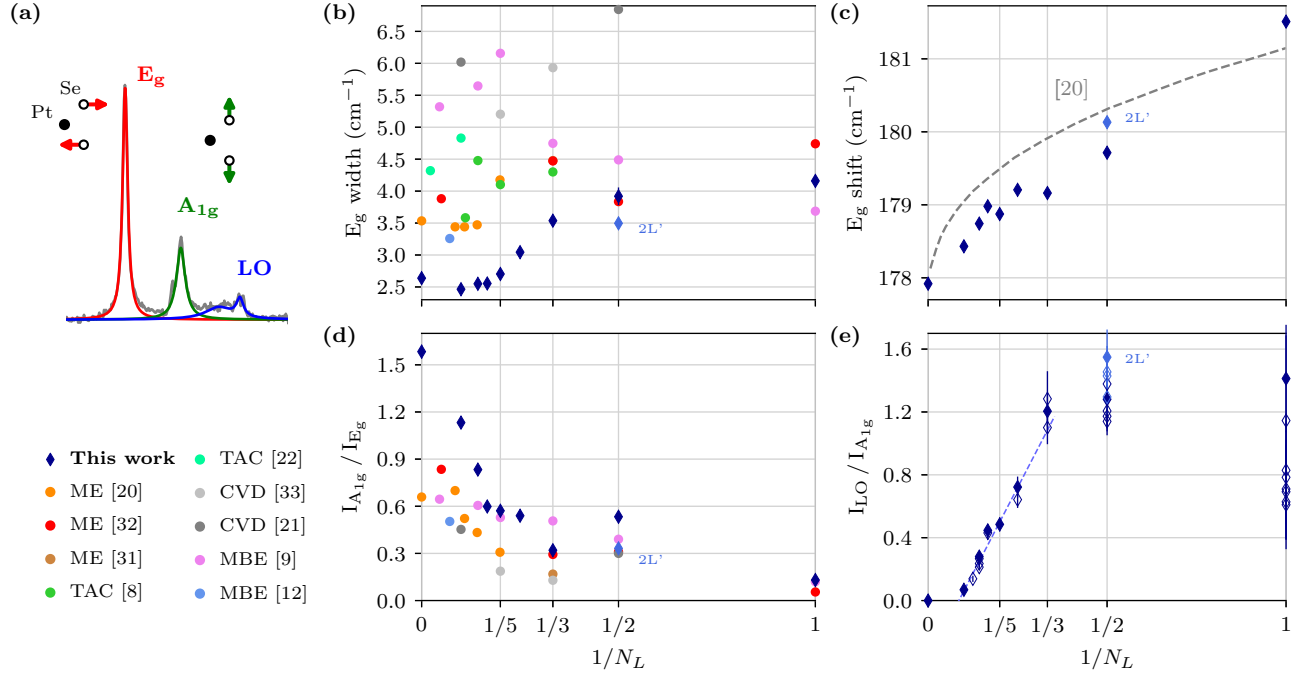


FIG. 2. Evolution of Raman spectra characteristics with layer count and film quality. (a) Decomposition of the 4-components Lorentzian fit into three contributions : E_g , A_{1g} and LO modes, and schematic of atomic motions for E_g and A_{1g} modes. (b) E_g peak width and (c) shift (the dashed line is a law derived from different studies in reference [20]). (d) Intensities ratio of A_{1g} to E_g modes and (e) LO to A_{1g} modes. Errorbars are included, displaying one standard deviation fitting uncertainty. The empty diamonds incorporate data not shown in figure 1, and the dashed line is a linear fit for 3 to 10 layers. For the sake of comparison, in (b) and (d) we reproduce digitalized Raman data from the literature [8, 9, 12, 20–22, 32–34], performed with green 532 nm or 514 nm light and where layer count is determined from film thickness considering an individual layer thickness of 0.5 nm [30]. 2L' is displayed in lighter blue to highlight the difference with other samples.

der Waals contact, due to the presence of interfacial layers of water [37].

CRYSTALLINE QUALITY

In TMDs and graphene, Raman mode linewidth is very sensitive to the defect level [14–17]. PtSe₂ is no exception, and the E_g linewidth has been shown to increase with film defectiveness [8, 20, 22]. For the 1L flakes studied in this work, a narrow E_g peak is associated with the presence

of sharp optical features in the absorption spectrum [30], again indicating the relevance of this Raman spectral signature.

Recent works reported the growth of good quality PtSe₂ films, using several methods: Thermally Assisted Conversion (TAC) [8, 22], Chemical Vapor Deposition (CVD) [21, 34] and Molecular Beam Epitaxy (MBE) [9, 12]. Some research focused instead on Mechanically Exfoliated (ME) PtSe₂ crystals [20, 32, 33]. These works stand out for their narrow E_g peaks (figure 2b), with linewidths values below 6 cm⁻¹ – reaching about 3.5 cm⁻¹ for thick ME, TAC and MBE samples, about 4 cm⁻¹ for ME and MBE 1L and 2L samples (however the film continuity of the MBE 1L is not established).

In our work, the high quality of the PtSe₂ flakes is assessed by the unprecedented narrow linewidth of this E_g mode, from monolayer to bulk thicknesses. The E_g linewidth reaches 4.2 cm⁻¹ for 1L, 3.9 cm⁻¹ for 2L and around 2.5 cm⁻¹ for thick samples (7L to bulk). Among the 1L exfoliated flakes studied, several feature large E_g linewidths (> 6 cm⁻¹), as shown in figure SM2. We could not identify if such flakes were damaged during the exfoliation process, or if they originated from more defective areas of the original CVT crystal. As reported by the aforementioned works, the E_g peak features of strong increase of its linewidth with decreasing film thickness (figure 2b). This increase is commonly attributed to increasing defectiveness as the film thickness diminishes [19].

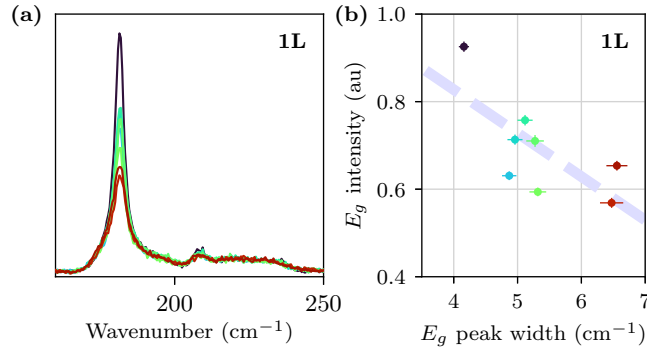


FIG. 3. E_g peak variability of monolayer samples. (a) Raman spectra, and (b) their E_g peak intensity versus width – the trend is given by a linear fit (dashed line). In both figures, the color represents the measured E_g linewidth.

Let us now turn our examination from the E_g peak width to its absolute intensity, which appears as a good criterion for film quality. Indeed, for a given layer count, the thin exfoliated PtSe₂ flakes

feature a large sample-to-sample variability of their E_g peak integrated intensities (figure 3a for the 1L case), while the A_{1g} and LO modes are unaffected. We observe that higher E_g peak intensity correlates with narrower linewidth (figure 3b, more thicknesses are studied in figure SM6), therefore appearing as a robust metric for film quality. This sensitivity of the E_g mode intensity to flake quality may be due to the high sensitivity to the electromagnetic environment and disorder of Fröhlich electron-phonon coupling which affects E longitudinal optical modes amplitudes in polar crystals [38, 39].

NUMBER OF LAYERS IDENTIFICATION

It is tempting to identify the number of layers from Raman signatures, in particular in PtSe₂ in which the strong thickness-dependence Raman spectra led several authors to propose metrics relying on the shift of the E_g peak or the ratio of A_{1g} to E_g peak intensity. In this section, we show that these methods are imprecise, and we propose a new method for exfoliated PtSe₂ crystals.

The E_g peak position exhibits a quasi-linear blueshift with the inverse number of layers $1 / N_L$. The observed dependency in figure 2c is qualitatively compatible with previous studies, compiled as a grey dashed line and proposed as a metric by reference [20]. However, the discrepancy between this metrics and our data is too large to allow layer count identification.

The A_{1g} to E_g peaks intensities is commonly considered as characteristic of the layer count [20, 40, 41]. Indeed the A_{1g} mode involves out-of-plane motion of external Se atoms (figure 2a) and its intensity rises with the thickness, while longitudinal optical LO modes disappear for high layer number [19]. These trends are observed as well in our work (figure 1b), but appear to be more complex for 1L and 2L. Nonetheless, the A_{1g} to E_g intensities ratio does not appear as a reliable signature of the layer count, as it differs significantly from one research to another (figure 2d, references therein). Moreover, as described above, we observe for low layer count important variations of the E_g peak intensity resulting in $I_{A_{1g}}/I_{E_g}$ dispersion.

We propose instead to identify the number of layers by using the A_{1g} and LO peaks which are more robust to the defect level. The A_{1g} to LO intensity ratio for each sample is represented in figure 2e, as a function of inverse number of layers $1/N_L$. One can see straight away that the thickness can be evaluated from 3 to 10 layers using the linear law displayed in figure 2e:

$$N_L = \frac{4.38}{I_{LO} / I_{A_{1g}} + 0.38} \quad (2)$$

Mono- and bi-layers are exceptions to this law, but can be easily identified. Both present similar A_{1g} and LO peaks intensities, and 1L has a remarkably low A_{1g} to E_g peaks intensities ratio, with $I_{A_{1g}}/I_{E_g} < 35\%$ with a singularly wide LO peak, while 2L has relatively high ratio $I_{A_{1g}}/I_{E_g} > 45\%$, and a sharper LO peak (figure SM2).

Beyond 10 layers, accurate determination of the layer count isn't critical anymore as AFM can provide a fair estimate.

CONCLUSION

By using exfoliated CVT PtSe₂ crystals with layer-defined thickness, this study provides reference Raman spectrographs of high-quality flakes, which are particularly important for benchmarking emerging high-quality growth methods. We showed that crystalline quality can be assessed from the width and height of the E_g mode peak, with E_g linewidth narrowing down to 4.2 cm^{-1} for monolayer and 2.5 cm^{-1} for thicker exfoliated PtSe₂. We observed that commonplace criteria for layer count identification, either based on E_g peak shift or on A_{1g} to E_g peaks intensities ratio, leaves much to be desired for exfoliated high-quality PtSe₂. This led us to propose a robust method in this latter case based on the A_{1g} and LO specific peaks pattern.

EXPERIMENTAL METHODS

Samples

A 60 nm gold film is deposited using evaporation on a fused silica substrate (QX/QS Quartz Suprasil 300 from Hellma Analytics), on which the crystals are pre-exfoliated. The samples are then annealed at 150°C and the gold film is peeled using thermal release tape, thereby detaching few-layer PtSe₂. The peeled gold film is then transferred to a target substrate, and the gold is removed using KI₂ etching.

Raman spectrometry

We use a Raman Qontor spectrometer from Renishaw with a 3000 gr/mm grating, a $\times 100$ microscope objective, a 514 nm laser source and a 50 cm^{-1} edgepass filter. The laser is operated at a power of $50\text{ }\mu\text{W}$, in order to suppress any thermal shift or broadening of the PtSe₂ lines (the spectral shift of the main E_g peak was evaluated to reach approximately $0.1\text{ cm}^{-1}/\text{mW}$). Each spectrum is integrated for 1 min and averaged 5 times. Muon peaks are eliminated from the spectra and the baseline is removed using a 3rd order polynomial fit of the background signal. The spectrometer is calibrated using a Si₁₀₀ crystal which possesses a Raman peak centered at 520.45 cm^{-1} [42].

ACKNOWLEDGEMENTS

The authors acknowledge the financial support from the European Union’s Horizon 2020 program under grant agreement no. 785219, no. 881603 (Core2 and 3 Graphene Flagship), as well as from ANR-2018-CE08-018-05 (BIRDS) and ANR-2021-CE24-0025 (ELuSeM).

DATA AVAILABILITY

The data that support the findings of this study are openly available, at [10.5281/zenodo.8256907](https://doi.org/10.5281/zenodo.8256907).

-
- [1] Y. Zhao, J. Qiao, Z. Yu, P. Yu, K. Xu, S. P. Lau, W. Zhou, Z. Liu, X. Wang, W. Ji, and Y. Chai, High-electron-mobility and air-stable 2d layered ptse2 fets, *Advanced Materials* **29**, 1604230 (2017), <https://onlinelibrary.wiley.com/doi/pdf/10.1002/adma.201604230>.
 - [2] F. Bonell, A. Marty, C. Vergnaud, V. Consonni, H. Okuno, A. Ouerghi, H. Boukari, and M. Jamet, High carrier mobility in single-crystal ptse2 grown by molecular beam epitaxy on zno(0001), *2D Materials* **9**, 015015 (2021).
 - [3] X. Yu, P. Yu, D. Wu, B. Singh, Q. Zeng, H. Lin, W. Zhou, J. Lin, K. Suenaga, Z. Liu, and Q. J. Wang, Atomically thin noble metal dichalcogenide: a broadband mid-infrared semiconductor, *Nature Communications* **9**, 1545 (2018).

- [4] R. A. B. Villaos, C. P. Crisostomo, Z.-Q. Huang, S.-M. Huang, A. A. B. Padama, M. A. Al-bao, H. Lin, and F.-C. Chuang, Thickness dependent electronic properties of pt dichalcogenides, [npj 2D Materials and Applications](#) **3**, 2 (2019).
- [5] A. Kandemir, B. Akbali, Z. Kahraman, S. V. Badalov, M. Ozcan, F. Iyikanat, and H. Sahin, Structural, electronic and phononic properties of ptse2: from monolayer to bulk, [Semiconductor Science and Technology](#) **33**, 085002 (2018).
- [6] Y. Ma, X. Shao, J. Li, B. Dong, Z. Hu, Q. Zhou, H. Xu, X. Zhao, H. Fang, X. Li, Z. Li, J. Wu, M. Zhao, S. J. Pennycook, C. H. Sow, C. Lee, Y. L. Zhong, J. Lu, M. Ding, K. Wang, Y. Li, and J. Lu, Electrochemically exfoliated platinum dichalcogenide atomic layers for high-performance air-stable infrared photodetectors, [ACS Applied Materials & Interfaces](#) **13**, 8518 (2021).
- [7] Z. Wang, Q. Li, F. Besenbacher, and M. Dong, Facile synthesis of single crystal ptse2 nanosheets for nanoscale electronics, [Advanced Materials](#) **28**, 10224 (2016), <https://onlinelibrary.wiley.com/doi/pdf/10.1002/adma.201602889>.
- [8] W. Jiang, X. Wang, Y. Chen, G. Wu, K. Ba, N. Xuan, Y. Sun, P. Gong, J. Bao, H. Shen, T. Lin, X. Meng, J. Wang, and Z. Sun, Large-area high quality ptse2 thin film with versatile polarity, [InfoMat](#) **1**, 260 (2019), <https://onlinelibrary.wiley.com/doi/pdf/10.1002/inf2.12013>.
- [9] M. Yan, E. Wang, X. Zhou, G. Zhang, H. Zhang, K. Zhang, W. Yao, N. Lu, S. Yang, S. Wu, T. Yoshikawa, K. Miyamoto, T. Okuda, Y. Wu, P. Yu, W. Duan, and S. Zhou, High quality atomically thin ptse2 films grown by molecular beam epitaxy, [2D Materials](#) **4**, 045015 (2017).
- [10] S. S. Han, J. H. Kim, C. Noh, J. H. Kim, E. Ji, J. Kwon, S. M. Yu, T.-J. Ko, E. Okogbue, K. H. Oh, H.-S. Chung, Y. Jung, G.-H. Lee, and Y. Jung, Horizontal-to-vertical transition of 2d layer orientation in low-temperature chemical vapor deposition-grown ptse2 and its influences on electrical properties and device applications, [ACS Applied Materials & Interfaces](#) **11**, 13598 (2019).
- [11] M. Hilse, K. Wang, and R. Engel-Herbert, Growth of ultrathin pt layers and selenization into ptse2 by molecular beam epitaxy, [2D Materials](#) **7**, 045013 (2020).
- [12] E. Desgué, P. Legagneux, *et al.*, High quality ptse2 films grown by molecular beam epitaxy for high frequency photodetection and optoelectronic mixing at 1.55 μm , Article in preparation (2023).
- [13] R. Gatensby, N. McEvoy, K. Lee, T. Hallam, N. C. Berner, E. Rezvani, S. Winters, M. O'Brien, and G. S. Duesberg, Controlled synthesis of transition metal dichalcogenide thin films for electronic applications, [Applied Surface Science](#) **297**, 139 (2014).

- [14] C. Neumann, S. Reichardt, P. Venezuela, M. Drögeler, L. Banszerus, M. Schmitz, K. Watanabe, T. Taniguchi, F. Mauri, B. Beschoten, S. V. Rotkin, and C. Stampfer, Raman spectroscopy as probe of nanometre-scale strain variations in graphene, [Nature Communications](#) **6**, 8429 (2015).
- [15] L. Banszerus, H. Janssen, M. Otto, A. Epping, T. Taniguchi, K. Watanabe, B. Beschoten, D. Neumaier, and C. Stampfer, Identifying suitable substrates for high-quality graphene-based heterostructures, [2D Materials](#) **4**, 025030 (2017).
- [16] S. Mignuzzi, A. J. Pollard, N. Bonini, B. Brennan, I. S. Gilmore, M. A. Pimenta, D. Richards, and D. Roy, Effect of disorder on raman scattering of single-layer MoS_2 , [Phys. Rev. B](#) **91**, 195411 (2015).
- [17] P. Maguire, D. S. Fox, Y. Zhou, Q. Wang, M. O'Brien, J. Jadwiszczak, C. P. Cullen, J. McManus, S. Bateman, N. McEvoy, G. S. Duesberg, and H. Zhang, Defect sizing, separation, and substrate effects in ion-irradiated monolayer two-dimensional materials, [Phys. Rev. B](#) **98**, 134109 (2018).
- [18] I. Stenger, L. Schué, M. Boukhicha, B. Berini, B. Plaçais, A. Loiseau, and J. Barjon, Low frequency raman spectroscopy of few-atomic-layer thick hbn crystals, [2D Materials](#) **4**, 031003 (2017).
- [19] M. O'Brien, N. McEvoy, C. Motta, J.-Y. Zheng, N. C. Berner, J. Kotakoski, K. Elibol, T. J. Pennycook, J. C. Meyer, C. Yim, M. Abid, T. Hallam, J. F. Donegan, S. Sanvito, and G. S. Duesberg, Raman characterization of platinum diselenide thin films, [2D Materials](#) **3**, 021004 (2016).
- [20] B. M. Szydłowska, O. Hartwig, B. Tywoniuk, T. Hartman, T. Stimpel-Lindner, Z. Sofer, N. McEvoy, G. S. Duesberg, and C. Backes, Spectroscopic thickness and quality metrics for ptse2 layers produced by top-down and bottom-up techniques, [2D Materials](#) **7**, 045027 (2020).
- [21] D. P. Gulo, H. Yeh, W.-H. Chang, and H.-L. Liu, Temperature-dependent optical and vibrational properties of ptse2 thin films, [Scientific Reports](#) **10**, 19003 (2020).
- [22] S. Lukas, O. Hartwig, M. Pechtl, G. Capraro, J. Bolten, A. Meledin, J. Mayer, D. Neumaier, S. Kataria, G. S. Duesberg, and M. C. Lemme, Correlating nanocrystalline structure with electronic properties in 2d platinum diselenide, [Advanced Functional Materials](#) **31**, 2102929 (2021), <https://onlinelibrary.wiley.com/doi/pdf/10.1002/adfm.202102929>.
- [23] S. Yin, W. Zhang, C. Tan, L. Chen, J. Chen, G. Li, H. Zhang, Y. Zhang, W. Wang, and L. Li, Thermal conductivity of few-layer pts2 and ptse2 obtained from optothermal raman spectroscopy, [The Journal of Physical Chemistry C](#) **125**, 16129 (2021).
- [24] I. Yasuda, T. Kawada, H. Matsumoto, M. Kawaguchi, and M. Hayashi, Helicity-resolved raman spectroscopy of mono- and a few-layers-thick ptse2, [Applied Physics Express](#) **16**, 053005 (2023).

- [25] J. Raczyński, E. Nowak, M. Nowicki, S. El-Ahmar, M. Szybowicz, and W. Koczorowski, Studies of temperature-dependent raman spectra of thin ptse2 layers on al2o3 substrate, *Materials Science and Engineering: B* **297**, 116728 (2023).
- [26] Hq graphene - ptse2, <https://www.hqgraphene.com/PtSe2.php> (2021).
- [27] S. B. Desai, S. R. Madhvapathy, M. Amani, D. Kiriya, M. Hettick, M. Tosun, Y. Zhou, M. Dubey, J. W. Ager III, D. Chrzan, and A. Javey, Gold-mediated exfoliation of ultralarge optoelectronically-perfect monolayers, *Advanced Materials* **28**, 4053 (2016), <https://onlinelibrary.wiley.com/doi/pdf/10.1002/adma.201506171>.
- [28] Y. Huang, Y.-H. Pan, R. Yang, L.-H. Bao, L. Meng, H.-L. Luo, Y.-Q. Cai, G.-D. Liu, W.-J. Zhao, Z. Zhou, L.-M. Wu, Z.-L. Zhu, M. Huang, L.-W. Liu, L. Liu, P. Cheng, K.-H. Wu, S.-B. Tian, C.-Z. Gu, Y.-G. Shi, Y.-F. Guo, Z. G. Cheng, J.-P. Hu, L. Zhao, G.-H. Yang, E. Sutter, P. Sutter, Y.-L. Wang, W. Ji, X.-J. Zhou, and H.-J. Gao, Universal mechanical exfoliation of large-area 2d crystals, *Nature Communications* **11**, 2453 (2020).
- [29] F. Liu, W. Wu, Y. Bai, S. H. Chae, Q. Li, J. Wang, J. Hone, and X.-Y. Zhu, Disassembling 2d van der waals crystals into macroscopic monolayers and reassembling into artificial lattices, *Science* **367**, 903 (2020), <https://www.science.org/doi/pdf/10.1126/science.aba1416>.
- [30] M. Tharrault, S. Ayari, E. Desgué, M. Arfaoui, R. L. Goff, P. Morfin, J. Palomo, M. Rosticher, S. Jaziri, B. Plaçais, P. Legagneux, F. Carosella, C. Voisin, R. Ferreira, and E. Baudin, The optical absorption in indirect semiconductor to semimetal ptse2 arises from direct transitions (2023), [arXiv:2311.01847 \[cond-mat.mtrl-sci\]](https://arxiv.org/abs/2311.01847).
- [31] L. Fang, W. Liang, Q. Feng, and S.-N. Luo, Structural engineering of bilayer ptse2 thin films: a first-principles study, *Journal of Physics: Condensed Matter* **31**, 455001 (2019).
- [32] T. Das, E. Yang, J. E. Seo, J. H. Kim, E. Park, M. Kim, D. Seo, J. Y. Kwak, and J. Chang, Doping-free all ptse2 transistor via thickness-modulated phase transition, *ACS Applied Materials & Interfaces* **13**, 1861 (2021), pMID: 33393295, <https://doi.org/10.1021/acsami.0c17810>.
- [33] S. Bae, S. Nah, D. Lee, M. Sajjad, N. Singh, K. M. Kang, S. Kim, G.-J. Kim, J. Kim, H. Baik, K. Lee, and S. Sim, Exciton-dominated ultrafast optical response in atomically thin ptse2, *Small* **17**, 2103400 (2021), <https://onlinelibrary.wiley.com/doi/pdf/10.1002/sml.202103400>.

- [34] H. Xu, H. Zhang, Y. Liu, S. Zhang, Y. Sun, Z. Guo, Y. Sheng, X. Wang, C. Luo, X. Wu, J. Wang, W. Hu, Z. Xu, Q. Sun, P. Zhou, J. Shi, Z. Sun, D. W. Zhang, and W. Bao, Controlled doping of wafer-scale ptse2 films for device application, *Advanced Functional Materials* **29**, 1805614 (2019), <https://onlinelibrary.wiley.com/doi/pdf/10.1002/adfm.201805614>.
- [35] L. Xu, H. Liu, C. Song, X. Li, F. Li, D. Li, L. Wang, X. Bai, and J. Qi, Evolution of interlayer stacking orders and rotations in bilayer ptse2 visualized by stem, *2D Materials* **8**, 025014 (2021).
- [36] G. H. Ryu, J. Chen, Y. Wen, and J. H. Warner, In-situ atomic-scale dynamics of thermally driven phase transition of 2d few-layered 1t ptse2 into ultrathin 2d nonlayered ptse crystals, *Chemistry of Materials* **31**, 9895 (2019).
- [37] H. Rokni and W. Lu, Direct measurements of interfacial adhesion in 2d materials and van der waals heterostructures in ambient air, *Nature Communications* **11**, 5607 (2020).
- [38] P. Y. Yu and M. Cardona, *Fundamentals of Semiconductors: Physics and Materials Properties* (Springer Berlin Heidelberg, Berlin, Heidelberg, 2010).
- [39] B. Miller, J. Lindlau, M. Bommert, A. Neumann, H. Yamaguchi, A. Holleitner, A. Högele, and U. Wurstbauer, Tuning the fröhlich exciton-phonon scattering in monolayer mos2, *Nature Communications* **10**, 807 (2019).
- [40] J. Shi, Y. Huan, M. Hong, R. Xu, P. Yang, Z. Zhang, X. Zou, and Y. Zhang, Chemical vapor deposition grown large-scale atomically thin platinum diselenide with semimetal–semiconductor transition, *ACS Nano* **13**, 8442 (2019).
- [41] W. Qiu, W. Liang, J. Guo, L. Fang, N. Li, Q. Feng, and S. N. Luo, Thickness-dependent ultrafast hot carrier and phonon dynamics of ptse2 films measured with femtosecond transient optical spectroscopy, *Journal of Physics D: Applied Physics* **54**, 075102 (2020).
- [42] N. Itoh and K. Shirono, Reliable estimation of raman shift and its uncertainty for a non-doped si substrate (nmij crm 5606-a), *Journal of Raman Spectroscopy* **51**, 2496 (2020), <https://analyticalsciencejournals.onlinelibrary.wiley.com/doi/pdf/10.1002/jrs.6003>.

Raman Spectroscopy of Monolayer to Bulk PtSe₂ Exfoliated Crystals - Supplementary Material

Marin Tharrault,¹ Eva Desgué,² Dominique Carisetti,² Bernard Plaçais,¹

Christophe Voisin,¹ Pierre Legagneux,² and Emmanuel Baudin^{1,3}

¹*Laboratoire de Physique de l'Ecole normale supérieure, ENS, Université PSL, CNRS,
Sorbonne Université, Université de Paris, 24 rue Lhomond, 75005 Paris, France*

²*Thales Research & Technology, 91767 Palaiseau, France*

³*Institut universitaire de France*

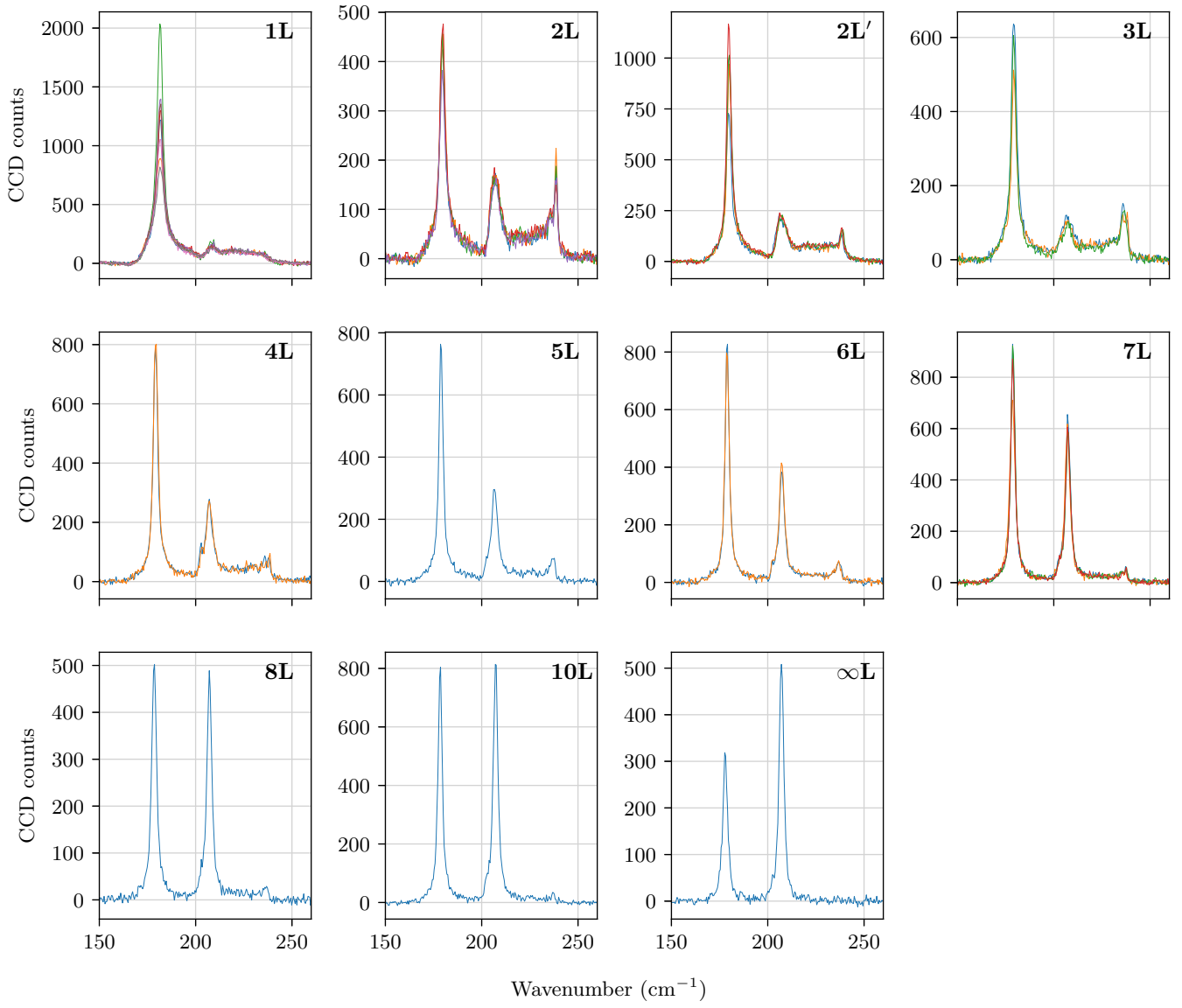


FIG. 1. Raw Raman spectra where the baseline has been substracted. Each spectrum originates from a different flake (for a total of 32 flakes).

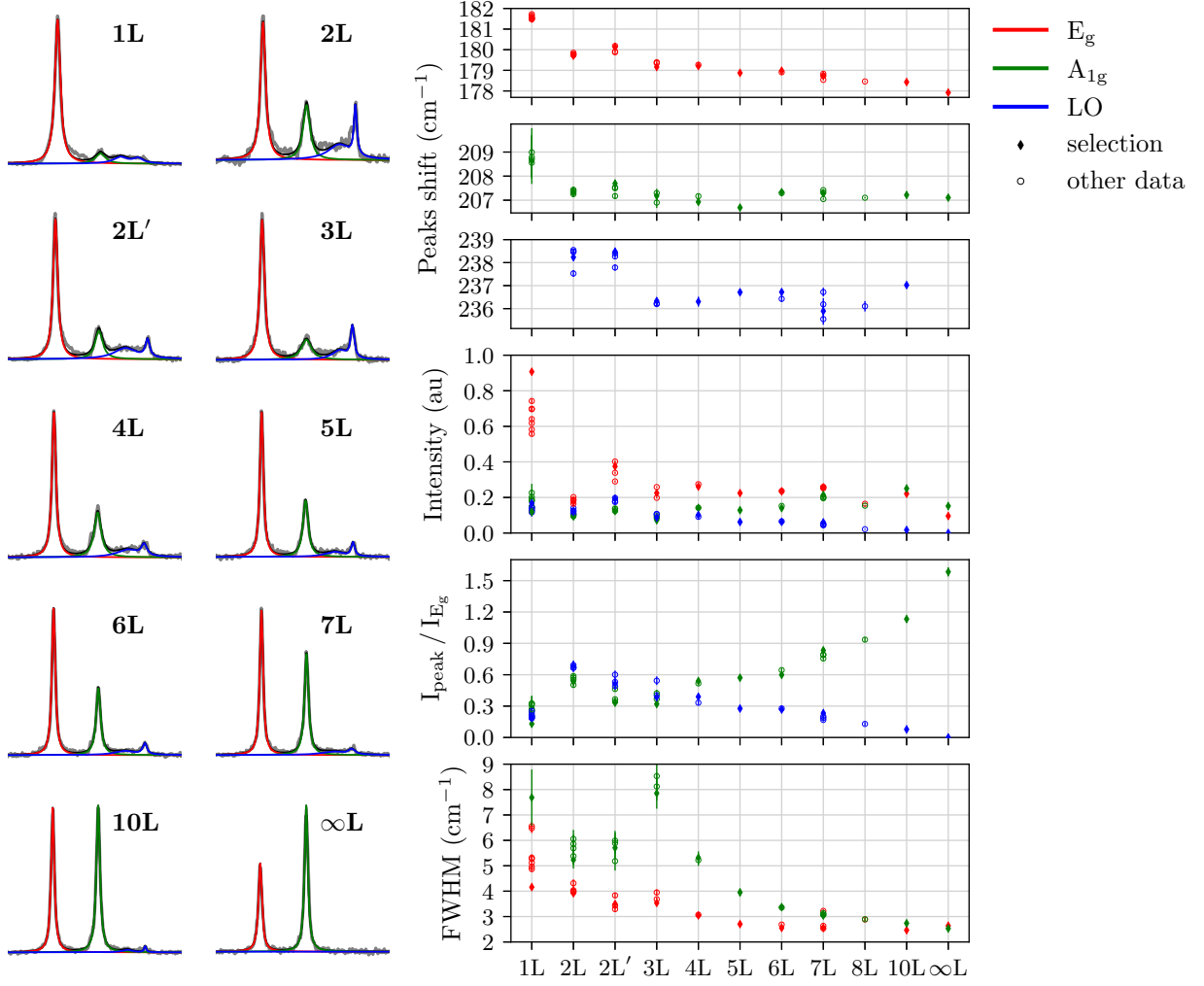


FIG. 2. Raman spectra peaks parameters. Left panel: selected spectra displayed in main text fig. 1 with the fit decomposition in E_g , A_{1g} and LO contributions in respectively red, green and blue. Right panel: The fit parameters extracted for all the measured spectra: peaks shifts, intensities, intensities ratios and full-width at half maximum (the LO peak shift refers to the position of the LO maximum amplitude). The selected spectra parameters are displayed as diamonds, and others as circles. Only well-fitted parameters are represented on these plots. Each datapoint is displaying a Raman mode parameter originating from a different flake. The fit is performed by attributing a $1/\sqrt{A}$ weight to each data point (A being the amplitude), to account for photon shot noise.

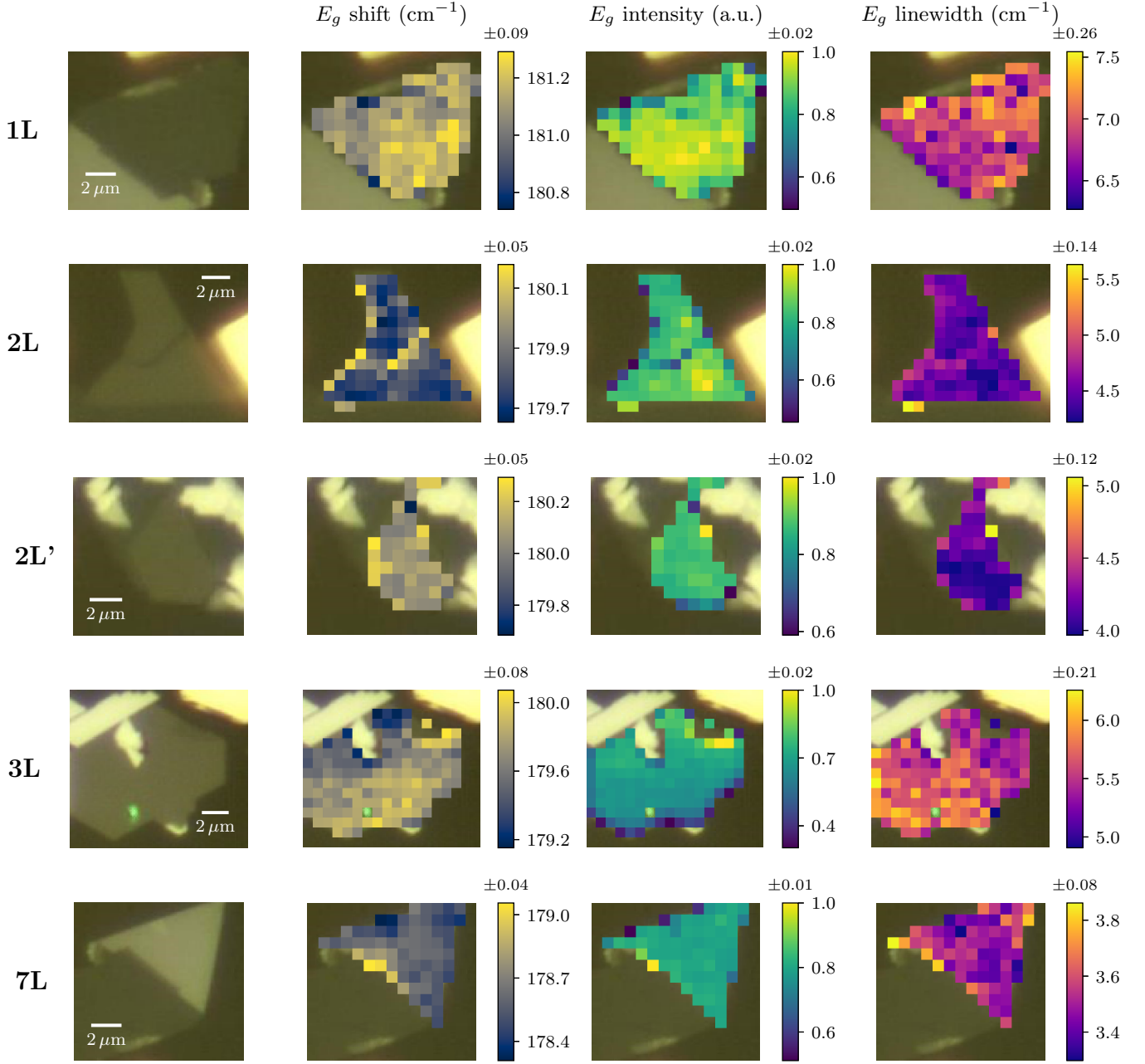


FIG. 3. Raman spectroscopy mappings of 1L, 2L, 2L', 3L and 7L flakes. The E_g mode shift, intensity and linewidth are extracted using the 4-components Lorentzian fit detailed in the main text. These quantities exhibit significant variations on the edges of the flakes, while they remain relatively uniform across the surface (within the fit standard deviation error, represented on top of each scale bar). For these measurements, a Raman Invia spectrometer (Renishaw) is used, with a $\sim 50\ \mu\text{W}$ 532 nm laser, 30 s integration time and a 1800 gr/mm grating.

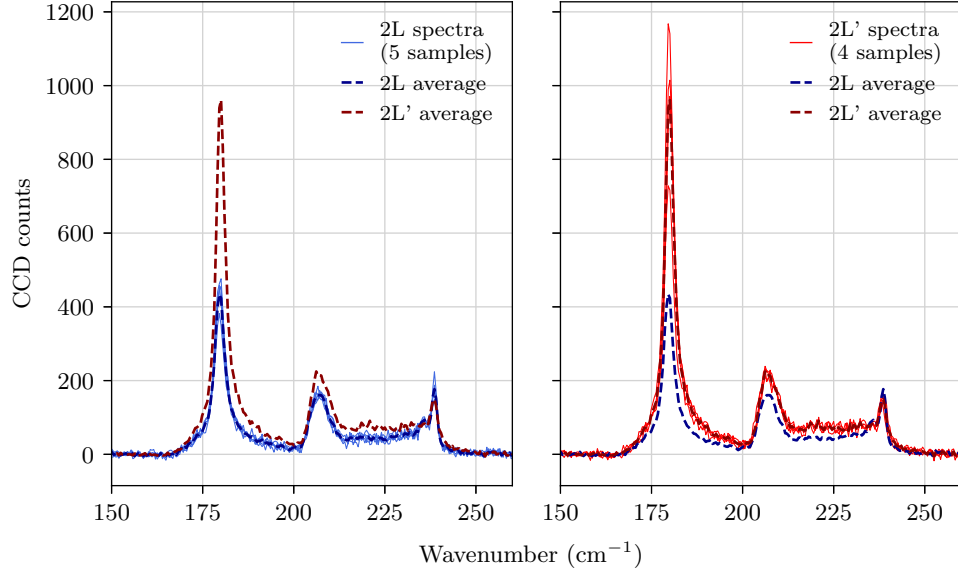


FIG. 4. Raman signatures of bilayer flakes, sorted as 2L (left) and 2L' (right). In dashed lines are represented the mean values of the 2L and 2L' spectra, highlighting that all bilayer samples can indeed be classified into these two categories.

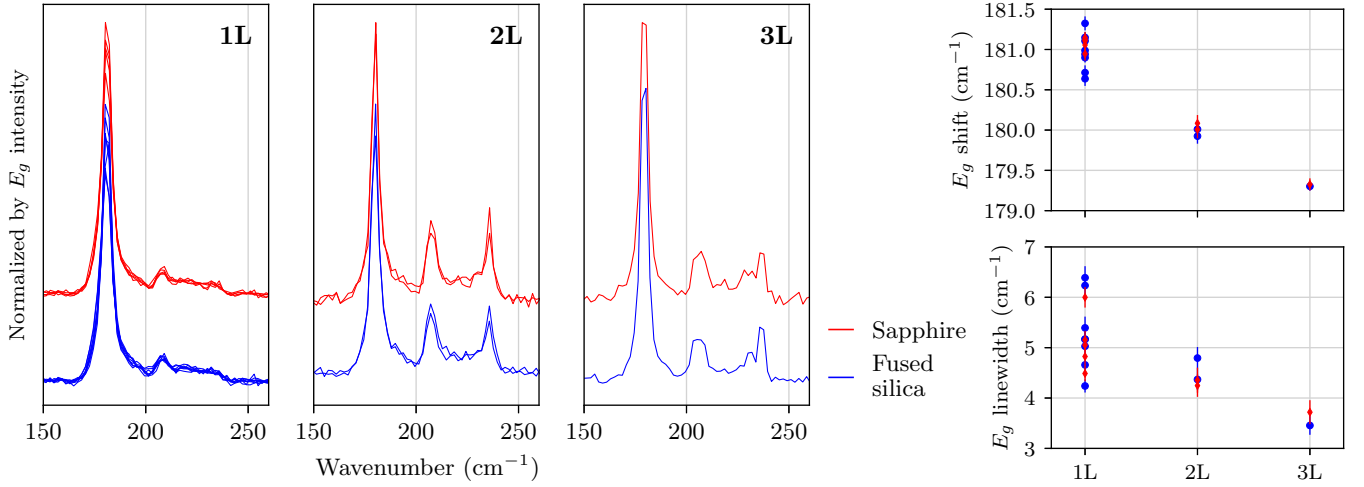


FIG. 5. Raman spectroscopy of 1L, 2L and 3L flakes on crystalline sapphire and on fused silica substrates. (left) Scattered Raman intensity, normalized by the E_g mode integrated intensity, and the (right) E_g mode shift and linewidth. A total of 8 flakes deposited on sapphire and 11 flakes deposited on fused silica have been inspected, respectively in red and blue. Raman signatures, E_g shifts and linewidths appear to be very similar. For these measurements, a Raman Invia spectrometer (Renishaw) is used, with a $\sim 50 \mu\text{W}$ 532 nm laser, 150 s integration time and a 1800 gr/mm grating.

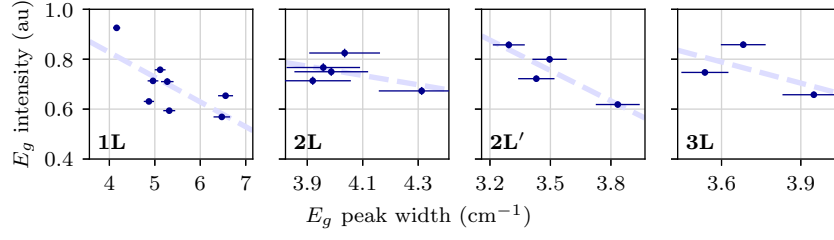


FIG. 6. E_g peak intensity correlation with its linewidth, for 1L, 2L, 3L – and 2L' bilayer flakes conjectured to originate from AB staking. The dashed lines are fitted, indicating the global trend. Each datapoint is originating from a different flake.